Article ID: 1006-8775(2019) 03-0324-12

DIURNAL CYCLES OF CONVECTIVE AND STRATIFORM PRECIPITATION OVER NORTH CHINA DURING SUMMER

ZHU Hao-ran (朱浩然), LI Xiao-fan (李小凡)
(Department of Atmospheric Sciences, School of Earth Sciences, Zhejiang University, Hangzhou 310027 China)

Abstract: The diurnal cycles of precipitation over northern China during summer in four strong rainfall years are examined using two-dimensional cloud-resolving modeling data. The diurnal signals are analyzed in terms of precipitation budget, fractional rainfall coverage and rain intensity over convective and stratiform rainfall area. The analysis of precipitation budget shows that the diurnal cycles of convective and stratiform precipitation mainly correspond respectively to those of water vapor convergence and transport of hydrometeor from convective rainfall area to stratiform rainfall area in 1964, 1994 and 1995, whereas they mainly correspond to those of water vapor convergence in 2013. The diurnal cycles of convective and stratiform precipitation are mainly associated with those of rain intensity in 1964, 1994 and 1995. In 2013, the diurnal cycle of stratiform precipitation is mainly related to that of fractional rainfall coverage over stratiform rainfall area. The multiple peaks of convective precipitation mainly correspond to the rain intensity maxima associated with strong water vapor convergence.

Key words: diurnal cycle; convective and stratiform precipitation; water vapor convergence; fractional rainfall convergence; rain intensity
CLC number: P456.7 **Document code:** A
doi: 10.16555/j.1006-8775.2019.03.004

1 INTRODUCTION

Over northern China, torrential rainfall often occurs during summertime, which causes severe floods and huge economic loss. Thus, accurate forecast is important for governmental decision making and has a strong impact on regional economic development. The development of torrential rainfall over northern China is associated with many factors and physical processes, including development of lower tropospheric low, shearline over warm sector and cold front over tropospheric trough (Ding et al. [1]), water vapor transport by southwesterly winds in mid-troposphere and by easterly winds in the lower troposphere (Liu et al.[2]), development of upper and lower tropospheric jets (Sun et al. [3]), western Pacific subtropical high (Tan and Sun [4]) and topographic effects on rainfall amplification (Sun [5]) and initiation of precipitation systems (Chen et al. [6]; Huang et al. [7]).

Diurnal cycle is one of the fundamental variabilities of precipitation systems. Duan et al. analyzed observational precipitation data from 2005 to 2007 using 2046 automatic weather stations over China and showed diurnal precipitation signals with primary nocturnal precipitation peak over northern China [8]. The physical mechanism that is responsible for nocturnal precipitation peak has been studied for half a century since Kraus [9]. Gray and Jacobson argued that nocturnal precipitation peak is induced by the radiational difference between clear-sky area and cloudy area[10]. Tao et al. suggested that the nocturnal precipitation maximum results from the increase in relative humidity [11]. Gao et al. and Gao and Li analyzed surface rainfall budget regarding water vapor and heat balance and found that the nocturnal infrared radiative cooling leads to the decrease in temperature and associated saturation mixing ratio, which enhances condensation and deposition and associated production of precipitation [12-13]. Dai used 3-hourly precipitation data from Global Telecommunication System (GTS) stations and from the Comprehensive Ocean-Atmosphere Data Set (COADS) to study the role of land-ocean contrast in the diurnal cycle of rainfall over the coastal areas and found that the land-ocean contrast accounts for the nocturnal rainfall peak[14].

Precipitation is associated with updrafts. Strong updrafts with inflows in the lower troposphere and outflows in the upper troposphere form deep convective cores throughout the troposphere, producing convective precipitation; the upper-tropospheric outflows advect ice hydrometeor form anvil clouds, produce stratiform precipitation while weak downward motions prevail in the lower troposphere. Thus, convective and stratiform precipitation are associated with the differences in

Received 2018-01-09; **Revised** 2019-05-06; **Accepted** 2019-08-15
Foundation item: National Natural Science Foundation of China (41775040, 41475039); National Key Basic Research and Development Project of China (2015CB953601)
Biography: LI Xiao-fan, Ph. D., Professor, primarily undertaking research on mesoscale meteorology and cloud microphysics.
Corresponding author: LI Xiao-fan, e-mail: xiaofanli@zju.edu.cn

vertical profiles of vertical velocity (Li et al. [15]), precipitation rate (Li et al. [16]), cloud microphysical processes (Cui et al.[17]), and radar reflectivity (Houze[18]).

Precipitation is associated with water vapor and cloud processes physically and its area mean is related to rain intensity and rainfall area naturally. Gao et al. and Cui and Li combined water vapor and cloud budgets to form surface precipitation budget and showed that precipitation rate is associated with water vapor processes including local water vapor change, water vapor convergence and surface evaporation and cloud processes including local hydrometeor change and hydrometeor convergence [19–20]. Cui analyzed diurnal cycle of rainfall using a two-dimensional equilibrium cloud-resolving model simulation data under zero large-scale vertical velocity and revealed that more water vapor convergence yields higher convective rain rate and more vapor convergence and more local vapor loss cause higher stratiform rain rate in early morning than in the afternoon [21]. By defining domain mean rain rate as a product of fractional rainfall coverage (FRC) and rain intensity (RI), Li et al. analyzed equilibrium model simulation data and found that the diurnal cycle of model domain mean rain rate is associated with that of FRC while the diurnal cycle of RI is much weaker due to the significant rainfall decrease in early morning hours[22].

Due to the lack of reliable observational data, the diurnal cycles of convective and stratiform rainfall over northern China has been seldom studied. The study of diurnal cycle of rainfall enhances understanding important processes that are responsible for the development of torrential rainfall over northern China. In this study, the diurnal cycles of torrential precipitation over northern China during summer are analyzed in convective and stratiform areas using month-long two-dimensional cloud-resolving model simulation data in selected years. The questions to be discussed in this study are: What are diurnal cycles of area-mean precipitation rate of northern China over convective and stratiform rainfall areas? Which dominant physical processes are responsible for diurnal cycles in precipitation budget? What is the relation between area-mean precipitation rate, rain intensity and fractional rainfall coverage at diurnal time scale? Model, data and numerical experiments are briefly introduced in the next section. The results are presented in section 3. The summary and discussion are given in section 4.

2 MODEL, DATA AND NUMERICAL EXPERIMENTS

A two-dimensional cloud-resolving model (Tao and Simpson [23]) is used in this study. The model is originally developed by Soong and Ogura [24] and Soong and Tao[25] for studying the formation and development of cloud-precipitation systems at hourly to daily time scales and modified by Sui et al.[26–27] for studying cloud-radiation interaction and environmental impacts on the production of precipitation at daily to monthly time scales. In this model setup, the horizontal boundary is periodic, and the model includes prognostic equations for perturbation momentum, potential temperature, specific humidity, and mixing ratios of cloud water, rain drops, cloud ice, snow and graupel. The model also has cloud microphysical parameterization schemes (Lin et al. [28]; Rutledge and Hobbs[29–30]; Tao et al.[31]; Krueger[32]) and solar and infrared radiative parameterization schemes (Chou et al. [33–36]). The horizontal domain is 768 km with 512 grid points and a horizontal grid resolution of 1.5 km. The vertical grid resolution ranges from about 200 m near the surface to about 1 km near 100 hPa. The time step is 12 s.

Precipitation data used in this study are provided by China International Ground Exchange Station. The data consist of 194 stations and are available from 1 January 1951 to 31 December 2014. The Japanese 55-year Reanalysis Data (JRA-55) (https://rda.ucar.edu/datasets/ds628.0/) are developed by Japan Meteorological Agency (JMA), which is based on a new data assimilation and prediction system (DA) that improves many deficiencies found in the first Japanese reanalysis. The horizontal resolution is 1.25° latitude by 1.25° longitude, the vertical resolution is 17 pressure levels and the time resolution is 6 hours.

The wind data used in this study come from the reanalysis data (http://www.esrl.noaa.gov/psd/data/gridded/data.ncep.reanalysis.pressure.html) developed by the National Center for Atmospheric Research (NCAR). The time resolution is 1 day and the horizontal resolution is 2.5° latitude by 2.5° longitude. There are 17 pressure levels from 1000 hPa to 10 hPa.

A small model domain cannot be used to simulate large-scale circulations. Thus, a large-scale forcing is required to force cloud-resolving model. The large-scale forcing includes vertical velocity, zonal wind, horizontal temperature, and water-vapor advection averaged in a rectangular box of 111 –119° E, 35 –37.5° N using JRA data from 0800 LST 1 July to 0800 LST 31 July. This rectangular box is chosen because of the maximum rainfall over northern China in July occurring within this area. We calculated monthly-mean precipitation data over a rectangular box of 111 –119° E, 35 –37.5° N using the 194-station data to analyze the precipitation over northern China and found that maximum precipitation occurs in July. Thus, the time series of July precipitation data from 1951 to 2014 is developed to calculate the time mean and standard deviation. The year in which July precipitation is larger than the mean plus standard deviation is considered strong precipitation year. Eight strong rainfall years (1962, 1964, 1969, 1977, 1988, 1990, 1994, 1995 and 2013) are identified. 1964, 1994, 1995 and 2013 are chosen for conducting cloud-resolving model simulations because large-scale forcing (upward motions) is consistent with observational precipitation. The other strong precipitation years are not chosen in this study because the large-scale upward motion and observed

precipitation are not consistent. The inconsistencies between large-scale upward motions and observed precipitation may be caused by the fact that the observed precipitation data are not assimilated to the reanalysis data used in this study, while the large-scale circulations are not properly simulated in the reanalysis system in those years. The vertical velocity in 1964, 1994, 1995 and 2013 is shown in Fig. 1. The upward motions occur in July 3–5, 12, 16, 26–27, 1964 (Fig. 1a), July 2–3, 5–6, 10–12, 1994 (Fig. 1b), July 10–11, 14–15, 17, 25, 1995 (Fig. 1c), and July 1–2, 3–4, 8–11, 12, 18, 22, 2013 (Fig. 1d).

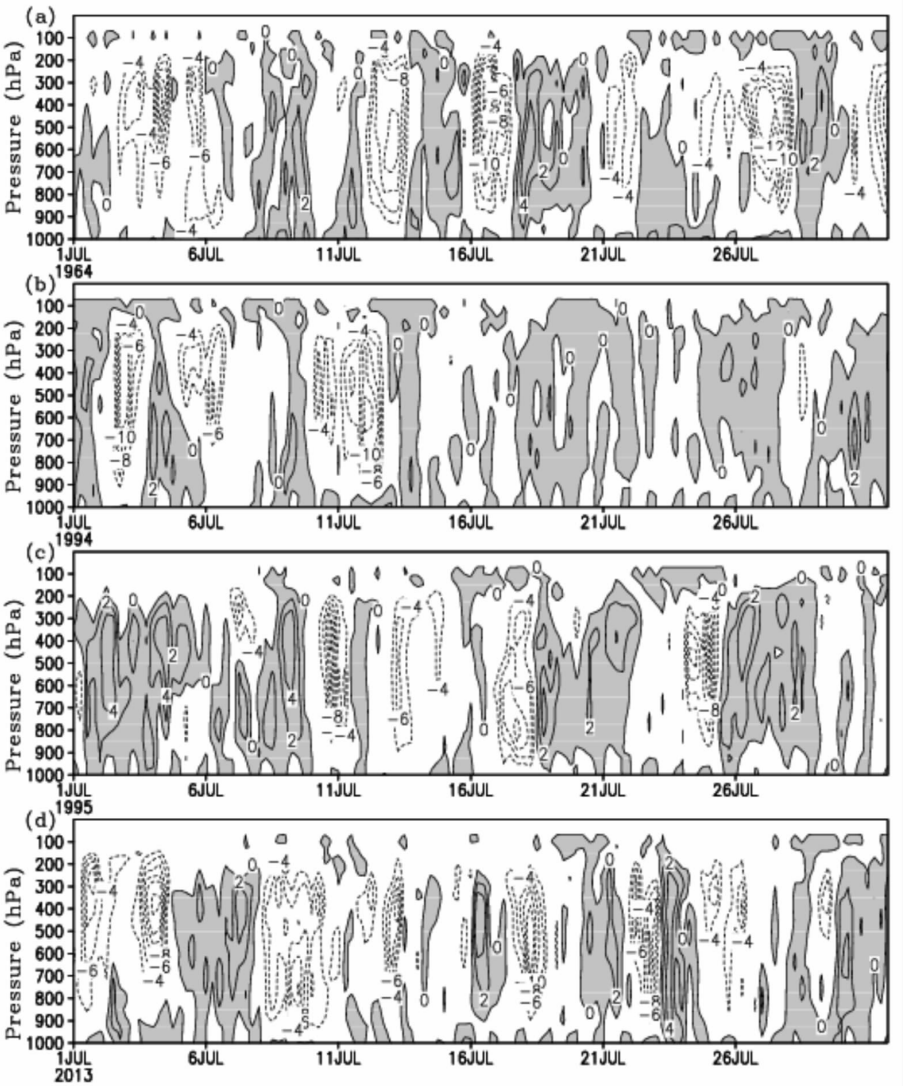

Figure 1. Temporal and vertical distribution of vertical velocity (unit: Pa s^{-1}) from 0800 LST 1 July to 0800 LST 31 July in (a) 1964, (b) 1994, (c)1995 and (d) 2013. Ascending motion is shaded. The data are averaged in a rectangular box (35–37.5°N, 111.25–128.75°E).

The model is integrated in about a month for each year. The simulated precipitation is compared with the observed precipitation using daily precipitation data. Fig. 2 shows that the observed precipitation is generally followed by the simulated precipitation, which is further demonstrated by the fact that the root-mean-squared difference (RMSD) is smaller than the standard deviation of observed precipitation (Table 1). The main difference appears in precipitation magnitude. The simulated precipitation is generally stronger than the observed precipitation in 1964 and 2013, whereas it is generally weaker than the observed precipitation in 1994 and 1995. The difference may stem from the accuracy of large-scale forcing from the reanalysis data and quality of observed precipitation data.

Table 1. The root mean squared difference (RMSD) between observed and simulated rain rate and the standard deviation (STD) of the observed rain rate. Unit is mm h^{-1}.

Year	1964	1994	1995	2013
RMS	6.63	5.06	6.31	7.92
STD	10.18	7.93	9.07	8.42

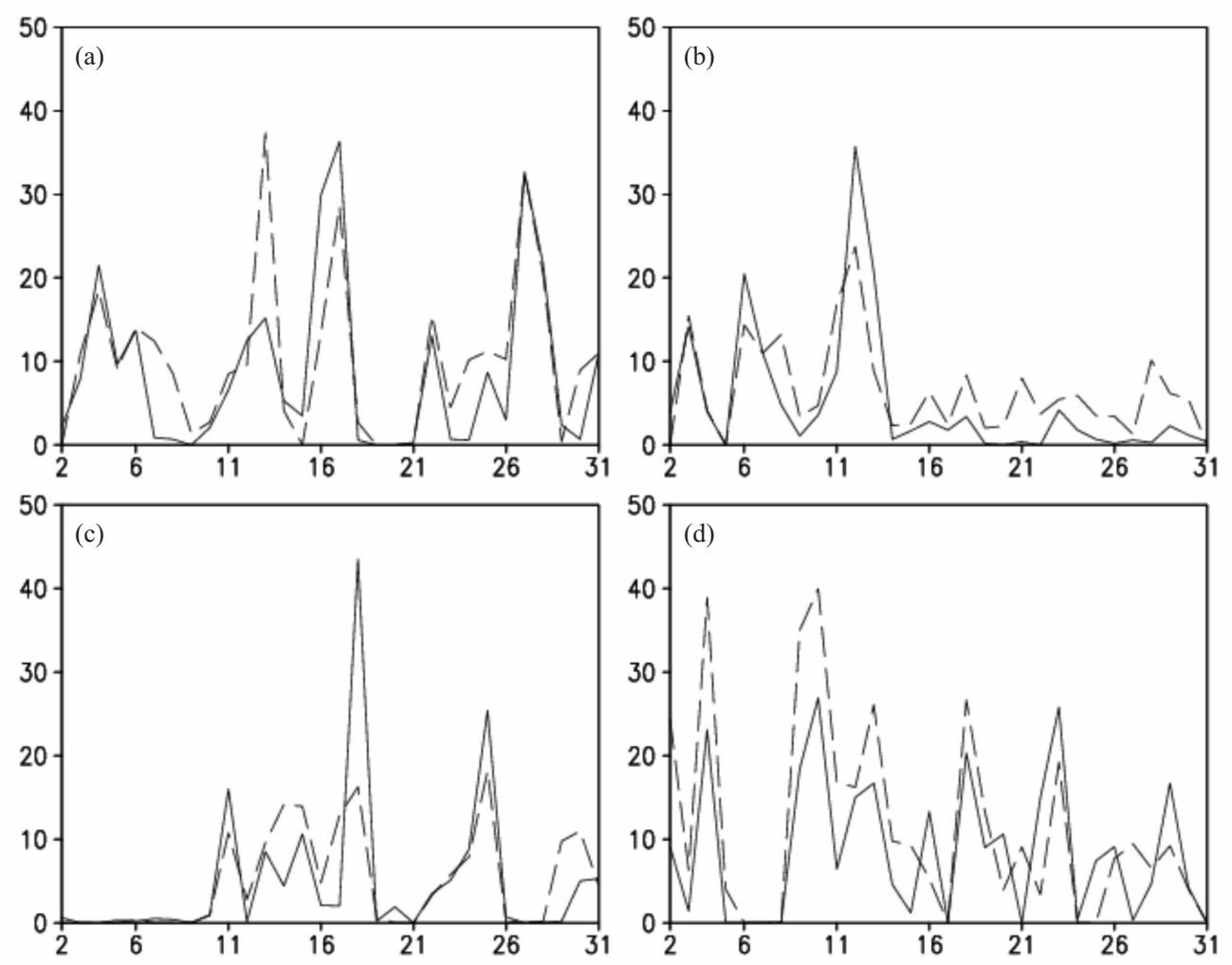

Figure 2. Time series of simulated (dashed lines) and observed (solid lines) surface rain rates (mm d^{-1}) in (a) 1964, (b) 1994, (c) 1995 and (d) 2013.

3 RESULTS

Precipitation consists of convective and stratiform components. Convective precipitation is different from stratiform precipitation in terms of precipitation intensity, vertical profiles of vertical velocity and cloud microphysical processes [15]. The convective-stratiform precipitation partitioning scheme used in this study is developed by Tao and Simpson [37] and modified by Sui et al. [26]. The scheme partitions surface rain rate in the two-dimensional *x*-*z* framework into convective or stratiform components based on the following main criteria. Model grid points in the surface rain-rate field that have a rain rate twice as large as the average taken over the surrounding four grid points (two grid points at the left and two grid points at the right) are identified as the cores of convective cells. For each core grid point, the one grid point on either side is also considered convective. In addition, any grid point with a rain rate of 20 mm h^{-1} or more is designated as convective regardless of the above criteria.

Convective precipitation is generally larger than stratiform precipitation in four years except in the first half of July of 2013 (Figs. 3 and 4), stratiform precipitation is dominant (Figs. 3d and 4d) when downward motions appear in the lower troposphere (Fig. 1d).

Precipitation is attributed to water vapor and cloud processes. Thus, precipitation budget is analyzed next. In precipitation budget, precipitation rate (P_S) can be expressed by

$$P_S = Q_{WVT} + Q_{WVF} + Q_{WVE} + Q_{CM}. \quad (1)$$

Here, Q_{WVT} is atmosphere drying (Q_{WVT}>0)/moistening (Q_{WVT}<0), QWVF is water vapor convergence (Q_{WVF}>0) /divergence (Q_{WVF}<0), Q_{WVE} is surface evaporation (Q_{WVE}>0) and Q_{CM} is hydrometeor loss/convergence (Q_{CM} >0) or hydrometeor gain/divergence (Q_{CM} <0).

The analysis of convective and stratiform precipitation shows: (1) Generally water vapor convergence occurs over convective precipitation area, forming a major source for convective precipitation, whereas water vapor divergence appears over stratiform

precipitation area; (2) Negative QCM over convective precipitation area and positive QCM over stratiform precipitation area denote the transport of cloud hydrometeor from convective precipitation area to stratiform precipitation area, forming a major source for stratiform precipitation; (3) Positive QWVT over both convective and stratiform precipitation areas indicates local atmospheric drying, contributing to convective and stratiform precipitation; (4) Surface evaporation rate is much smaller than other precipitation processes over both convective and stratiform precipitation areas; (5) In the first half of July 2013, stratiform precipitation is mainly associated with water vapor convergence over stratiform precipitation area (Fig. 4d).

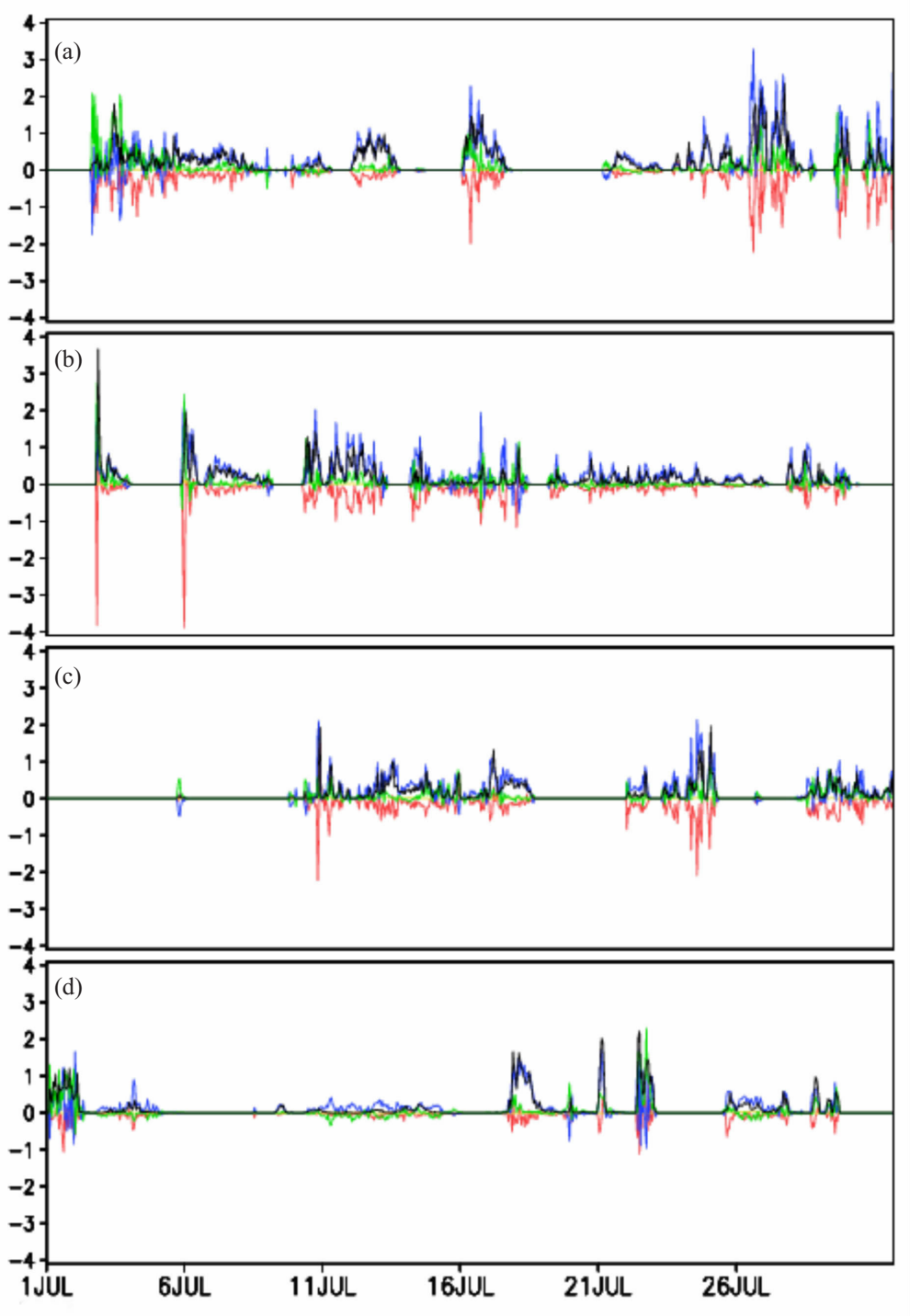

Figure 3. Time series of surface rainfall budget [PS (black), QWVT (green), QWVF (blue), QWVE (yellow) and QCM (red)] over convective rainfall area in (a) 1964, (b) 1994, (c) 1995 and (d) 2013. Unit is mmh^{-1}.

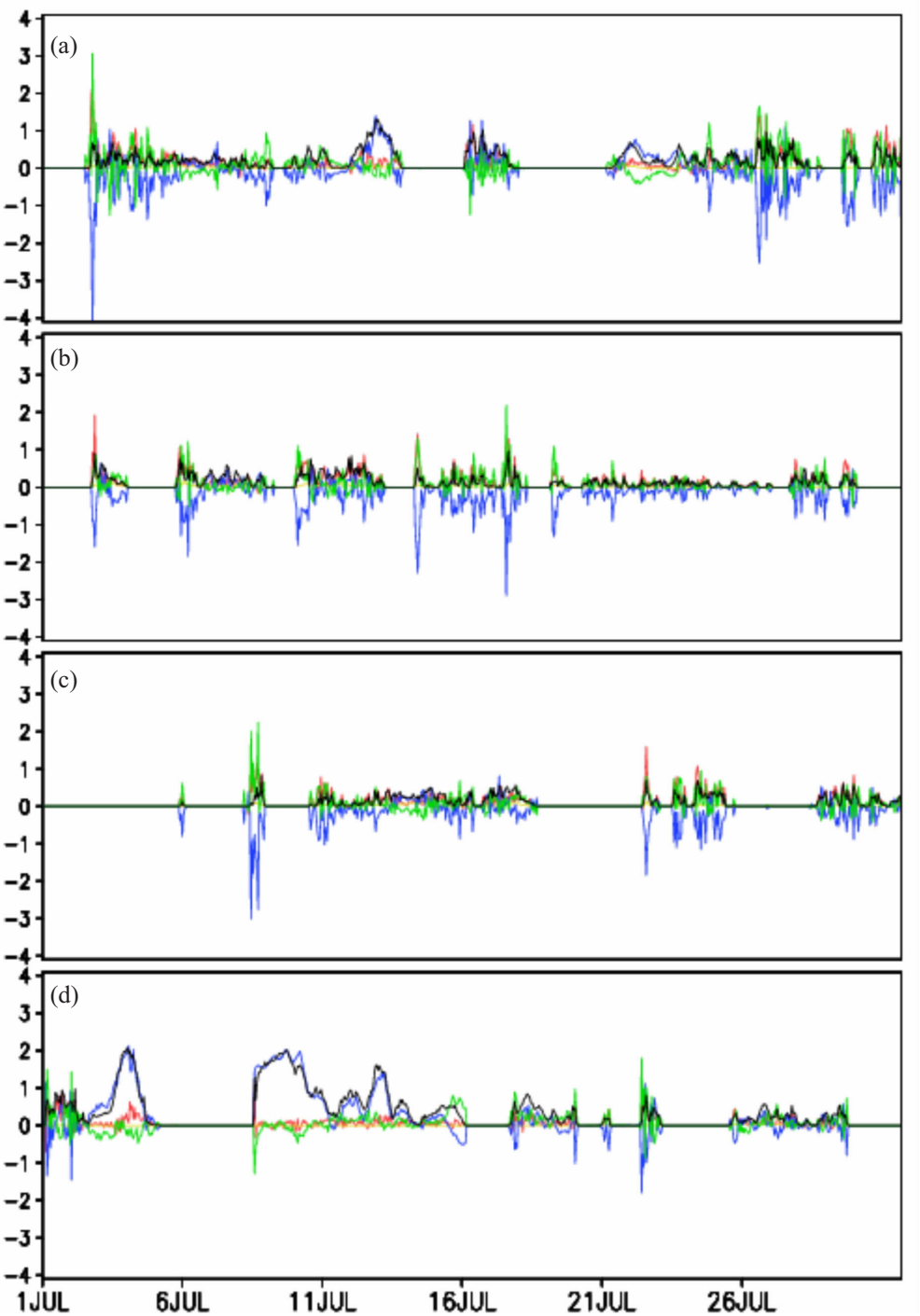

Figure 4. The same as Fig. 3 except for those over stratiform rainfall area.

Hourly precipitation data are composited to form diurnal cycles of precipitation for both convective and stratiform precipitation budgets (Figs. 5 and 6). Maximum convective precipitation occurs at hour 1 in 1964, hour 5 in 1994, hour 6 in 1995 and 2013 (Fig. 5), indicating that convective precipitation peaks generally occur in early morning, which is consistent with those found by Duan et al.[8] in their analysis of surface automatic weather station precipitation data from 2005 to 2007. A precipitation maximum also appears around 11 in 2013. The analysis of convective precipitation budget reveals that nocturnal convective precipitation peak is mainly attributed to water vapor convergence and local atmospheric drying over convective rainfall area. The water vapor convergence is usually associated with the large-scale circulation-induced water vapor transport, whereas the local atmospheric drying corresponds to the increase in condensation and deposition caused by the increase in relative humidity associated with the nocturnal infrared radiative cooling [12−13]. The local atmospheric drying

generally shows larger magnitudes during nighttime than during daytime, suggesting clear diurnal signals associated with the diurnal signals of solar radiative heating during daytime and infrared radiative cooling during nighttime. Since the large-scale forcing prescribed in this study may contain diurnal radiative signals, the diurnal signals of water vapor convergence are weaker than those of local atmospheric drying.

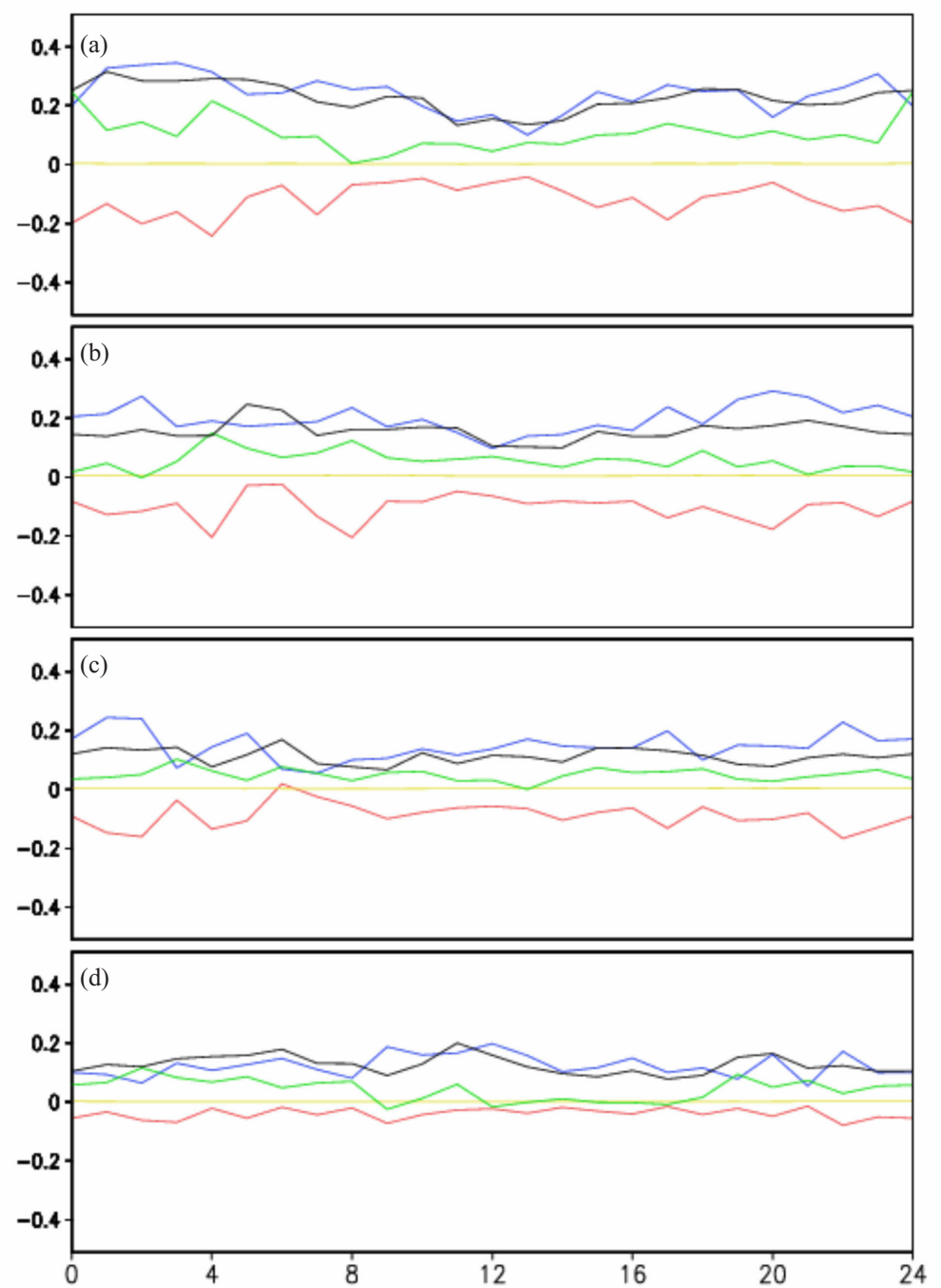

Figure 5. Diurnal composites of surface rainfall budget [P_S (black), Q_{WVT} (green), Q_{WVF} (blue), Q_{WVE} (yellow) and Q_{CM} (red)] over convective rainfall area in (a) 1964, (b) 1994, (c) 1995 and (d) 2013. Unit is mm h^{-1}.

Maximum stratiform precipitation appears around hours 2−5 in 1964, at hours 0 and 5 in1994, around hours 22−8 in 1995 and hours 3−7 in 2013 (Fig. 6). Nocturnal stratiform precipitation peaks are mainly associated with the transport of hydrometeor from convective rainfall areas to stratiform rainfall areas as well as local atmospheric drying over stratiform rainfall areas in 1964, 1994 and 1995. In contrast, the nocturnal stratiform precipitation maximum in 2013 corresponds mainly to the water vapor convergence over stratiform rainfall area, while the transport of hydrometeor from convective rainfall areas to stratiform rainfall areas and local atmospheric drying over stratiform rainfall areas are much less important.

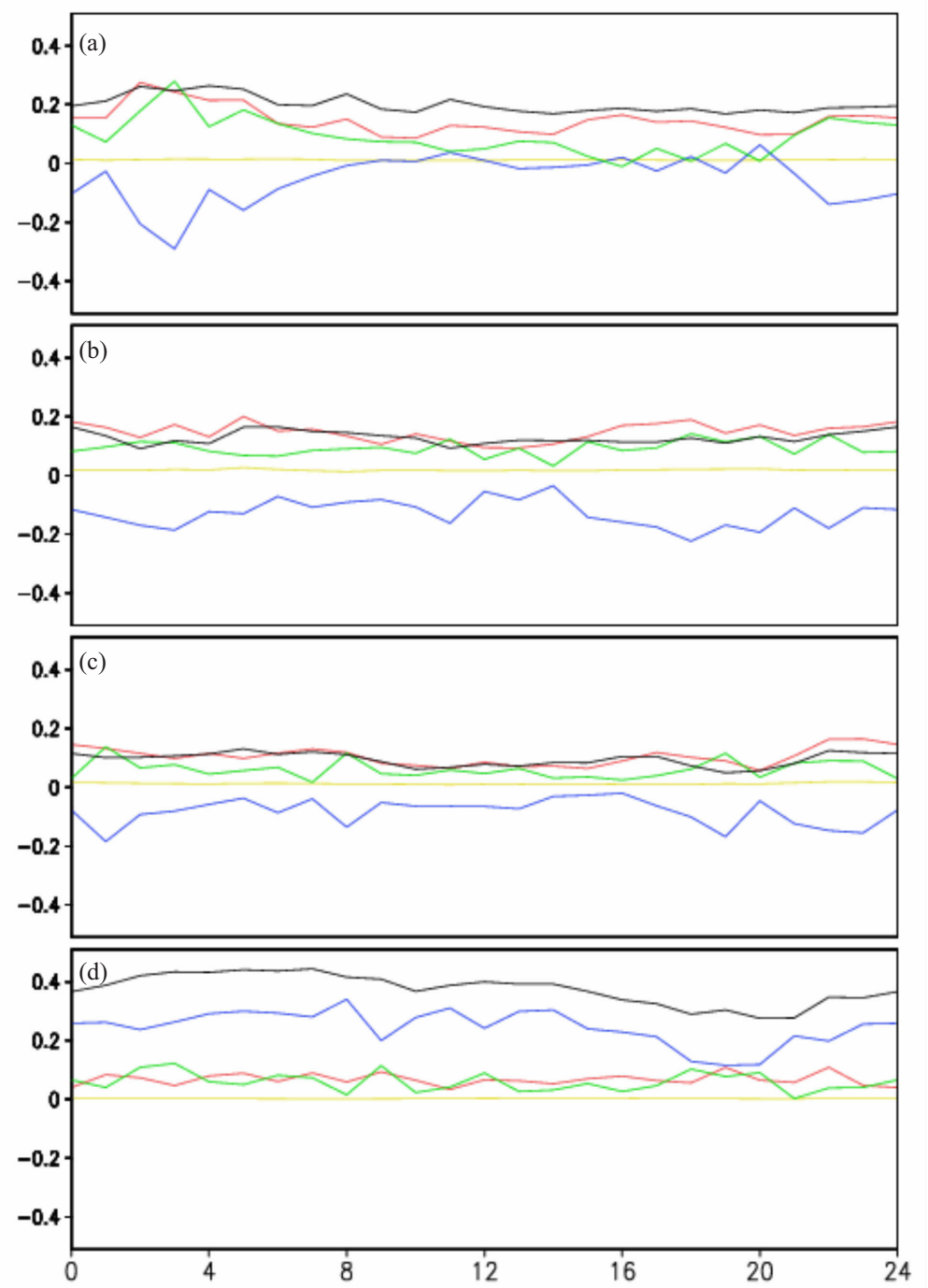

Figure 6. The same as Fig. 5 except for those over stratiform rainfall area.

To examine the relation between area mean rain rate, FRC and RI at diurnal time scale, we compute diurnal composites of area mean rain rate, FRC and RI over both convective and stratiform rainfall areas. FRC is calculated by dividing rainfall area over model domain, and RI is computed by averaging rain rate over rainfall area.

The diurnal cycles of convective precipitation in 1964, 1994 and 1995 are mainly associated with those of RI while the diurnal signal of FRC is not significant (Fig. 7). In 1964, the RI peaks appear around hours 2–6. The RI peak at hour 2 contributes to maximum convective precipitation peak. In 1994, the RI peaks occur at hours 4, 6 and 8. In 1995, the RI peak contributes to convective precipitation peak at hour 3. In 2013, FRC shows a significant diurnal signal with its maximum at hour 5 and its minimum at hour 15. Maximum convective precipitation at hour 11 is related to maximum RI.

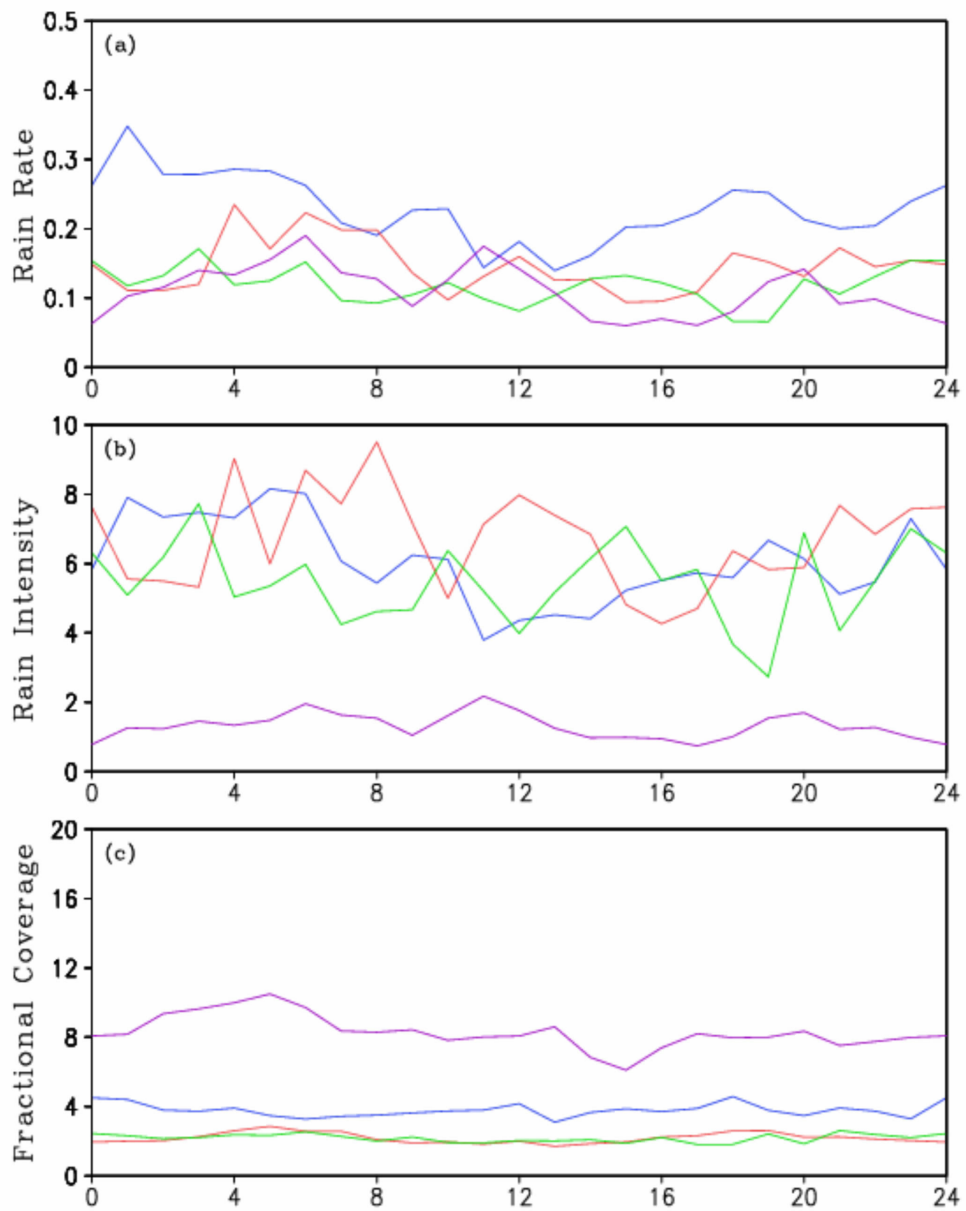

Figure 7. Diurnal composites of (a) area mean rain rate, (b) rain intensity and (c) fractional rainfall coverage in year 1964 (blue), 1994 (red), 1995 (green) and 2013 (purple) over convective rainfall area. Unit is mm h^{-1} for rain rate and rain intensity and % for fractional rainfall coverage.

The diurnal cycles of stratiform precipitation in 1964 and 2013 are mainly associated with those of FRC (Fig. 8). The FRC peaks appear around hours 0–4 in 1964 and at hour 2 in 2013. The diurnal cycles of stratiform precipitation in 1994 and 1995 are mainly associated with those of RI while the diurnal signals of FRC are less important. The stratiform precipitation peaks in 1994 mainly correspond to the maximum RIs around hours 4–8. The stratiform precipitation maximum in 1995 results from the RI maximum at hour 3.

4 SUMMARY AND DISCUSSIONS

Diurnal cycles of convective and stratiform precipitation over northern China in July of four strong precipitation years (1964, 1994, 1995 and 2013) are examined through the analyses of precipitation budget and fraction rainfall coverage/rain intensity. The month-long precipitation events are simulated with a two-dimensional cloud-resolving model and the simulations are compared with observational rainfall data. The fair agreement between the simulations and observations allow the simulations for the analysis of diurnal cycles.

Both convective and stratiform precipitation generally shows diurnal signals in 1964, 1994 and 1995. The diurnal cycles of convective precipitation correspond to those of water vapor convergence and local atmospheric drying over convective rainfall area, whereas

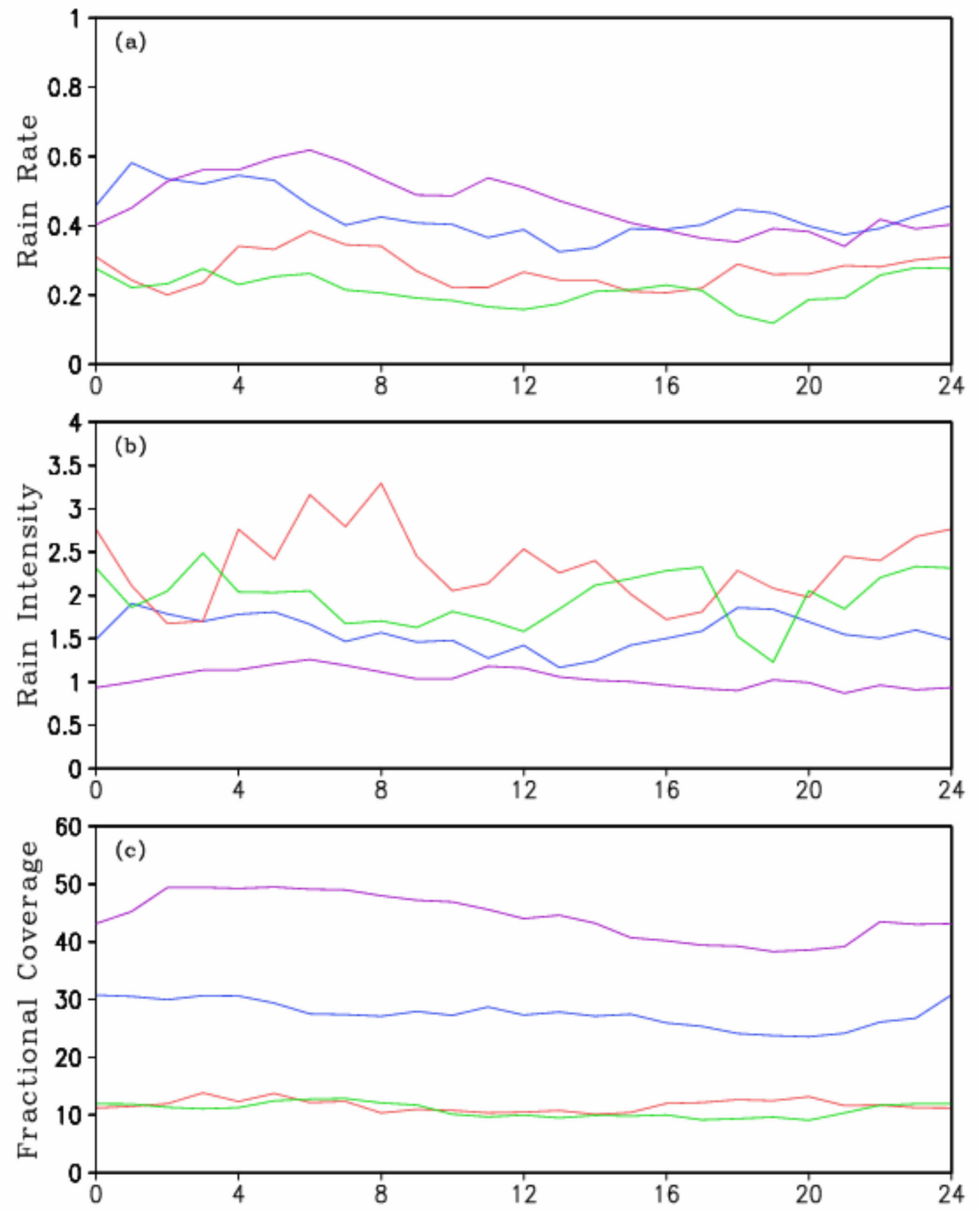

Figure 8. The same as Fig. 7 except for those over stratiform rainfall area.

the diurnal cycles of stratiform precipitation are associated with those of transport of hydrometeor from convective rainfall area to stratiform rainfall area and local atmospheric drying. Nocturnal peaks of local atmospheric drying over both convective and stratiform rainfall areas imply radiative effects on rainfall, which is related to the consumption of water vapor to condensation and deposition as a result of the increase in relative humidity due to infrared radiative cooling. The difference in major precipitation resources between diurnal signals of convective and stratiform precipitation indicates large-scale forcing. In 2013, the diurnal cycle of stratiform precipitation is mainly related to that of water vapor convergence. The convective precipitation peaks around noon and evening mainly correspond to maximum water vapor convergence.

Diurnal cycles of convective and stratiform precipitation are also examined by analyzing diurnal signals of fractional rainfall coverage and rain intensity. The results reveal that diurnal cycles of convective and stratiform precipitation are mainly associated with those of rain intensity in 1964, 1994 and 1995. In 2013, fractional rainfall coverage of both convective and stratiform rainfall area show diurnal signals with nocturnal maxima. The diurnal cycle of stratiform precipitation corresponds to that of fractional rainfall coverage over stratiform rainfall area, whereas multiple rain-intensity peaks over convective rainfall area contribute to multiple maxima of convective precipitation. The analysis suggests that diurnal cycle of rain intensity may be determined by water vapor convergence whereas the diurnal variation of fractional

rainfall coverage may be controlled by local atmospheric drying associated with radiative effects.

Acknowledgement: The authors thank the support from the Training Center of Atmospheric Sciences of Zhejiang University.

REFERENCES:

[1] DING Y H, LI J S, SUN S Q. The analysis on mesoscale systems producing heavy rainfall in north China [C]. Papers of Institute of Atmospheric Physics, Chinese Academy of Sciences, 1980, 9: 1-13 (in Chinese).

[2] LIU Ang-ran, GUO Da-min, XIN Bao-heng, et al. Some aspects of water vapor associated with "75.7" torrential rainfall over north China [J]. Acta Meteor Sin, 1979, 37 (2): 79-82 (in Chinese).

[3] SUN Jian-hua, QI Lin-lin, ZHAO Si-xiong. A study on mesoscale convective systems of the severe heavy rainfall in north China by "9608" Typhoon [J]. Acta Meteor Sin, 2006, 64(1): 57-71 (in Chinese).

[4] TAN G, SUN Z. Relationship of the subtropical high and summertime floods/droughts over north China [J]. J Trop Meteor, 2004, 20(2): 206-211 (in Chinese).

[5] SUN J. The effects of vertical distribution of the lower level flow on precipitation location [J]. Plat Meteor, 2005, 24(1): 62-69 (in Chinese).

[6] CHEN S, WANG Y, ZHANG W, et al. Intensifying mechanism of the convective storm moving from the mountain to the plain over Beijing area [J]. Meteor Mon, 2011, 37(7): 802-813 (in Chinese).

[7] HUANG R, WANG Y, ZHANG W. Initiating and intensifying mechanism of a local thunderstorm over complex terrain of Beijing [J]. Torrential Rain and Disasters, 2012, 31(4): 232-241 (in Chinese).

[8] DUAN C, CAO W, MIAO Q, et al. Spatial distribution of night rainfall in summer over China [J]. J Nat Res, 2013, 28(11): 1935-1944.

[9] KRAUS E B. The diurnal precipitation change over the sea [J]. J Atmos Sci, 1963, 20(6): 551-556.

[10] GRAY W M, JACOBSON R W. Diurnal variation of deep cumulus convection [J]. Mon Wea Rev, 1977, 105 (9): 1171-1188.

[11] TAO W K, LANG S, SIMPSON J, et al. Mechanism of cloud-radiation interaction in the tropics and midlatitude [J]. J Atmos Sci, 1996, 53(18): 2624-2651.

[12] GAO S, CUI X, LI X. A modeling study of diurnal rainfall variations during the 21-day period of TOGA COARE [J]. Adv Atmos Sci, 2009, 26(5): 895-905.

[13] GAO S, LI X. Precipitation equations and their applications to the analysis of diurnal variation of tropical oceanic rainfall [J]. J Geophys Res, 2010, 115(D08), doi: 10.1029/2009JD012452.

[14] DAI A. Global precipitation and thunderstorm frequencies, Part II: Diurnal variations [J]. J Climate, 2001, 14(5): 1112-1128.

[15] LI X, ZHAI G, GAO S, et al. A new convective-stratiform rainfall separation scheme [J]. Atmos Sci Lett, 2014, 15(4): 245-251.

[16] LI X, SUI C H, LAU K M. Dominant cloud microphysical processes in a tropical oceanic convective system: A 2-D cloud resolving modeling study [J]. Mon Wea Rev, 2002, 130(10): 2481-2491,

[17] CUI X, ZHU Y, LI X. Cloud microphysical properties in tropical convective and stratiform regions [J]. Meteor Atmos Phys, 2007, 98(1): 1-11.

[18] HOUZE R A Jr. Stratiform precipitation in region of convection: A meteorological paradox? [J] Bull Amer Meteor Soc, 1997, 78(10): 2179-2196.

[19] GAO S, CUI X, ZHOU Y, et al. Surface rainfall processes as simulated in a cloud-resolving model [J]. J Geophys Res, 2005, 110 (D10), doi: 10.1029/2004JD005467.

[20] CUI X, LI X. Role of surface evaporation in surface rainfall processes [J]. J Geophys Res, 2006, 111 (D17), doi:10.1029/2005JD006876.

[21] CUI X. A cloud-resolving modeling study of diurnal variations of tropical convective and stratiform rainfall [J]. J Geophys Res, 2008, 113 (D02), doi: 10.1029/2007JD008990.

[22] LI X, ZHAI G, ZHU P, et al. An equilibrium cloud-resolving modeling study of diurnal variation of tropical rainfall [J]. Dyn Atmos Oceans, 2015, 71 (1): 108-117.

[23] TAO W K, SIMPSON J. The Goddard cumulus ensemble model, Part I: Model description [J]. Terr Atmos Oceanic Sci, 1993, 4(1): 35-72.

[24] SOONG S T, OGURA Y. Response of tradewind cumuli to large-scale processes [J]. J Atmos Sci, 1980, 37 (9): 2035-2050.

[25] SOONG S T, TAO W K. Response of deep tropical cumulus clouds to mesoscale processes [J]. J Atmos Sci, 1980, 37(9): 2016-2034.

[26] SUI C H, LAU K M, TAO W K, et al. The tropical liquid and energy cycles in a cumulus ensemble model, Part I: Equilibrium climate [J]. J Atmos Sci, 1994, 51 (5): 711-728.

[27] SUI C H, LI X, LAU K M. Radiative-convective processes in simulated diurnal variations of tropical oceanic convection [J]. J Atmos Sci, 1998, 55 (14): 2345-2359.

[28] LIN Y L, FARLEY R D, ORVILLE H D. Bulk parameterization of the snow field in a cloud model [J]. J Climate Appl Meteor, 1983, 22(6): 1065-1092.

[29] RUTLEDGE S A, HOBBS P V. The mesoscale and microscale structure and organization of clouds and precipitation in midlatitude cyclones, Part VIII: A model for the "seeder-feeder" process in warm-frontal rainbands [J]. J Atmos Sci, 1983, 40(5): 1185-1206.

[30] RUTLEDGE S A, HOBBS P V. The mesoscale and microscale structure and organization of clouds and precipitation in midlatitude cyclones, Part XII: A diagnostic modeling study of precipitation development in narrow cold-frontal rainbands [J]. J Atmos Sci, 1984, 41(20): 2949-2972.

[31] TAO W K, SIMPSON J, McCUMBER M. An ice-liquid saturation adjustment [J]. Mon Wea Rev, 1989, 117(1): 231-235.

[32] KRUEGER S K, FU Q, LIOU K N, et al. Improvement of an ice-phase microphysics parameterization for use in numerical simulations of tropical convection [J]. J Appl Meteor, 1995, 34(1): 281-287.

[33] CHOU M D. A solar radiation model for use in climate studies [J]. J Atmos Sci, 1992, 49(9): 762-772.

[34] CHOU M D, SUAREZ M J. An efficient thermal infrared radiation parameterization for use in general circulation models [EB]. NASA Tech Memo 104606(3), 1994: 1-85, https://www.researchgate.net/publication/2329334_An_Efficient_Thermal_Infrared_Radiation_Parameterization_For_Use_In_General_Circulation_Models.

[35] CHOU M D, KRATZ D P, RIDGWAY W. Infrared radiation parameterization in numerical climate models [J]. J Climate, 1991, 4(4): 424-437.

[36] CHOU M D, SUAREZ M J, HO C H, et al. Parameterizations for cloud overlapping and shortwave single scattering properties for use in general circulation and cloud ensemble models [J]. J Atmos Sci, 1998, 55 (2): 201-214.

[37] TAO W K, SIMPSON J, SUI C H, et al. Heating, moisture and liquid budgets of tropical and midlatitude squall lines: Comparisons and sensitivity to longwave radiation [J]. J Atmos Sci, 1993, 50(5): 673-690.

Citation: ZHU Hao-ran and LI Xiao-fan. Diurnal cycles of convective and stratiform precipitation over north China during summer [J]. J Trop Meteor, 2019, 25(3): 324-335.